THE JOURNAL OF PHYSICAL CHEMISTRY Letters

Letter

Ultrafast Structural Evolution and Chromophore Inhomogeneity Inside a Green Fluorescent Protein Based Ca Biosensor

Longteng Tang, Weimin Liu, Yanli Wang, Liangdong Zhu, Fangyuan Han, and Chong Fang

J. Phys. Chem. Lett., **Just Accepted Manuscript** • DOI: 10.1021/acs.jpclett.6b00236 • Publication Date (Web): 16 Mar 2016

ACS Publications

The Journal of Physical Chemistry Letters is published by the American Chemical Society. 1155 Sixteenth Street N.W., Washington, DC 20036

Ultrafast Structural Evolution and Chromophore Inhomogeneity Inside a Green Fluorescent Protein Based Ca^{2+} Biosensor

*Longteng Tang, Weimin Liu, Yanli Wang, Liangdong Zhu, Fangyuan Han,[†] and Chong Fang**

Department of Chemistry, Oregon State University, Corvallis, Oregon 97331, United States

[†]Current address: Guangxi Power Grid Electric Power Research Institute, Nanning, Guangxi 530023, China

Corresponding Author

*E-mail: Chong.Fang@oregonstate.edu. Phone: 541-737-6704.

ABSTRACT. Understanding excited state structural dynamics of fluorescent-protein-based biosensors for Ca^{2+} imaging is crucial for developing new in-vivo Ca^{2+} indicators and advancing bioimaging. We implemented wavelength-tunable femtosecond stimulated Raman spectroscopy (FSRS) with a 530-nm Raman pump to uncover the working mechanism of an intensiometric fluorescent-protein biosensor, G-GECO1.1, highlighting the deprotonation process of its embedded chromophore. Besides confirming the dynamic difference of excited-state proton transfer (ESPT) in the Ca^{2+}-free/bound protein, we revealed a chromophore two-ring twisting process with time constants of 36/60 ps that competes with ESPT. In contrast to FSRS data collected using the 800-nm Raman pump, the bluer Raman pump enables us to access a subset of reactant population with partially deprotonated character that exhibits an additional ESPT component on the ~5-ps timescale. These findings provide deep mechanistic insights into the inhomogeneity and subpopulation-specific conformational dynamics of biosensor chromophores, which will guide the rational design of improved biosensors for metal ion imaging.

TOC GRAPHICS

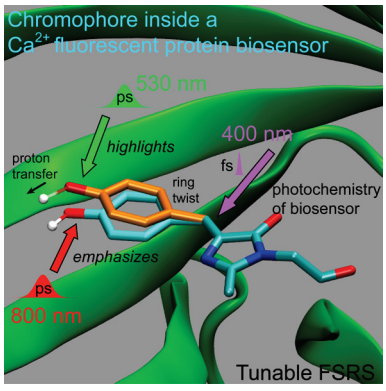

KEYWORDS. Ca^{2+} biosensor, green fluorescent protein, ultrafast vibrational spectroscopy, excited-state proton transfer, chromophore ring twist, tunable femtosecond stimulated Raman

The discovery of green fluorescent protein (GFP) as a genetically encodable bioimaging marker[1-3] has revolutionized molecular and cellular biology and greatly facilitated bioengineering and biomedical advances.[4-6] Because GFP is highly tolerant to structural manipulations, protein engineers have successfully converted FPs to a large number of FP derivatives and FP-based biosensors. Since the 1990s, the extension of FPs to sensitively detect the target analyte in cellular environment such as metal ions and adenosine triphosphate (ATP) has gained momentum and yielded important results.[3,7-9] One of the exciting directions is the development of biosensors that track calcium ions (Ca^{2+}), which play a vital role in the function of all mammalian cells including neuron activity and cancer metastasis.[10,11] G-GECO1.1, a recently developed intensiometric FP-based Ca^{2+} biosensor with a Thr-Tyr-Gly (TYG) chromophore,[12,13] exhibits more than two-fold fluorescence intensity change upon Ca^{2+} binding when compared to its GFP-calmodulin (CaM) predecessor GCaMP3.[13-15] The protonated TYG chromophores in both the Ca^{2+}-free and bound biosensors emit green photons upon 400-nm photoexcitation via excited-state proton transfer (ESPT) from its phenolic hydroxyl to adjacent proton acceptors.

In our previous report,[16] we used femtosecond stimulated Raman spectroscopy (FSRS) with 800-nm Raman pump[17-20] to probe photoinduced proton transfer reaction coordinate of the chromophore inside the protein pocket. After the impulsively driven wavepackets move out of the Franck-Condon region, an ESPT time constant of ~50 ps in the Ca^{2+}-free biosensor shortens to ~30 ps in the Ca^{2+}-bound biosensor. The calcium ions induce conformational changes of the CaM domain that reposition Arg377 at the interfacial region, resulting in a more hydrophilic environment for the embedded FP-chromophore. However, as the photoexcited protonated chromophore (A*) converts to the deprotonated chromophore in the excited state (I*), the 800-nm Raman pump cannot probe I* species with high enough signal-to-noise ratio due to changes

in the resonance Raman condition.[17,21,22] Therefore, structural evolution from A* to I* could not be fully monitored. Whether or not the chromophore undergoes a notable conformational change along the ESPT reaction coordinate remains unresolved. In order to provide deep insights into the photochemistry of G-GECO1.1 biosensor chromophore, we developed a tunable FSRS setup (see Supporting Information, Figure S1) with 530-nm Raman pump[23] to access a different region of the excited-state potential energy surface, aiming to elucidate the conformational dynamics of the TYG chromophore beyond the initial A* decay following 400-nm photoexcitation.

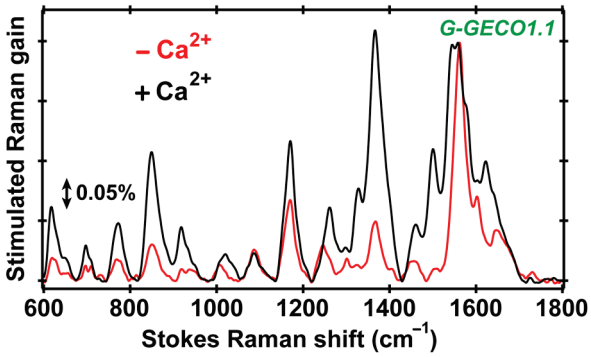

Figure 1. Ground-state FSRS of the G-GECO1.1 biosensor with 530-nm Raman pump. The Ca^{2+}-free/bound sample is shown in red/black solid curves, respectively. The Ca^{2+}-bound sample spectrum is scaled by a factor of 0.51 to match the Ca^{2+}-free sample peak at ~1560 cm^{-1}. The double-arrowed line indicates an absolute stimulated Raman gain of 0.05%.

We first performed ground-state (S_0) FSRS for the Ca^{2+}-free/bound biosensors. The overall spectral pattern in Figure 1 is similar for both samples, mostly arising from the three-residue chromophore that senses the light stimulus. Since about 1/6 of the chromophores are deprotonated following Ca^{2+} binding (see Supporting Information, Figure S2)[24] while the 530-nm Raman pump wavelength is much closer to the absorption peak of the deprotonated form in S_0 (B state) at ~500 nm, the Raman mode intensities for the Ca^{2+}-bound biosensor are much stronger

than those in the Ca^{2+}-free biosensor with similar sample concentrations. After normalizing to the 1560 cm^{-1} mode intensity, the 1366 cm^{-1} mode exhibits additional enhancement in the Ca^{2+}-bound state, which indicates that the polarizability of the corresponding normal mode is significantly increased in the deprotonated chromophore. Aided by density functional theory (DFT) calculations in Gaussian,[25] we assigned major atomic motions to the observed vibrational modes in S_0 between ca. 600—1700 cm^{-1} (see Supporting Information, Table S1/S2 for the Ca^{2+}-free/bound biosensor chromophore, respectively). Comparisons between ground-state spectra collected with the 530-nm Raman pump and those with the 800-nm Raman pump (Supporting Information, Figure S3) supports significant enhancement of deprotonated chromophore Raman signal strength using a visible pump. The observed mode frequency shift indicates that different chromophore species are being specifically enhanced by different Raman pump wavelengths.

After subtracting the ground-state FSRS, the time-resolved excited-state Raman spectra are stack-plotted in Figure 2 (see baselines in Figure S4). Unlike our FSRS data with 800-nm Raman pump[16] wherein all the modes diminish after ~120 ps, the Raman modes here show distinct temporal evolution. We reported the ~1370 cm^{-1} I* mode[16] gradually rising in Ca^{2+}-free/bound biosensor spectra, and confirmed the ESPT time difference. In addition, there are new transient A* and I* modes revealed by tunable FSRS between ca. 600—1700 cm^{-1} (Figure 2). For instance, a pronounced redshift of the 1180 cm^{-1} mode correlates with the increase of the 1370 cm^{-1} mode intensity. This phenomenon was not observed in FSRS with 800-nm Raman pump wherein the 1176 cm^{-1} mode frequency remains unchanged between ~200 fs and 650 ps (detection time window limited by the length of our 10-cm translation stage). Moreover, the ~1400 cm^{-1} mode emerges promptly following photoexcitation that decays away with the rise of the ~1370 cm^{-1} mode of I* on the 42/22 ps timescale in the Ca^{2+}-free/bound biosensor, respectively.[16]

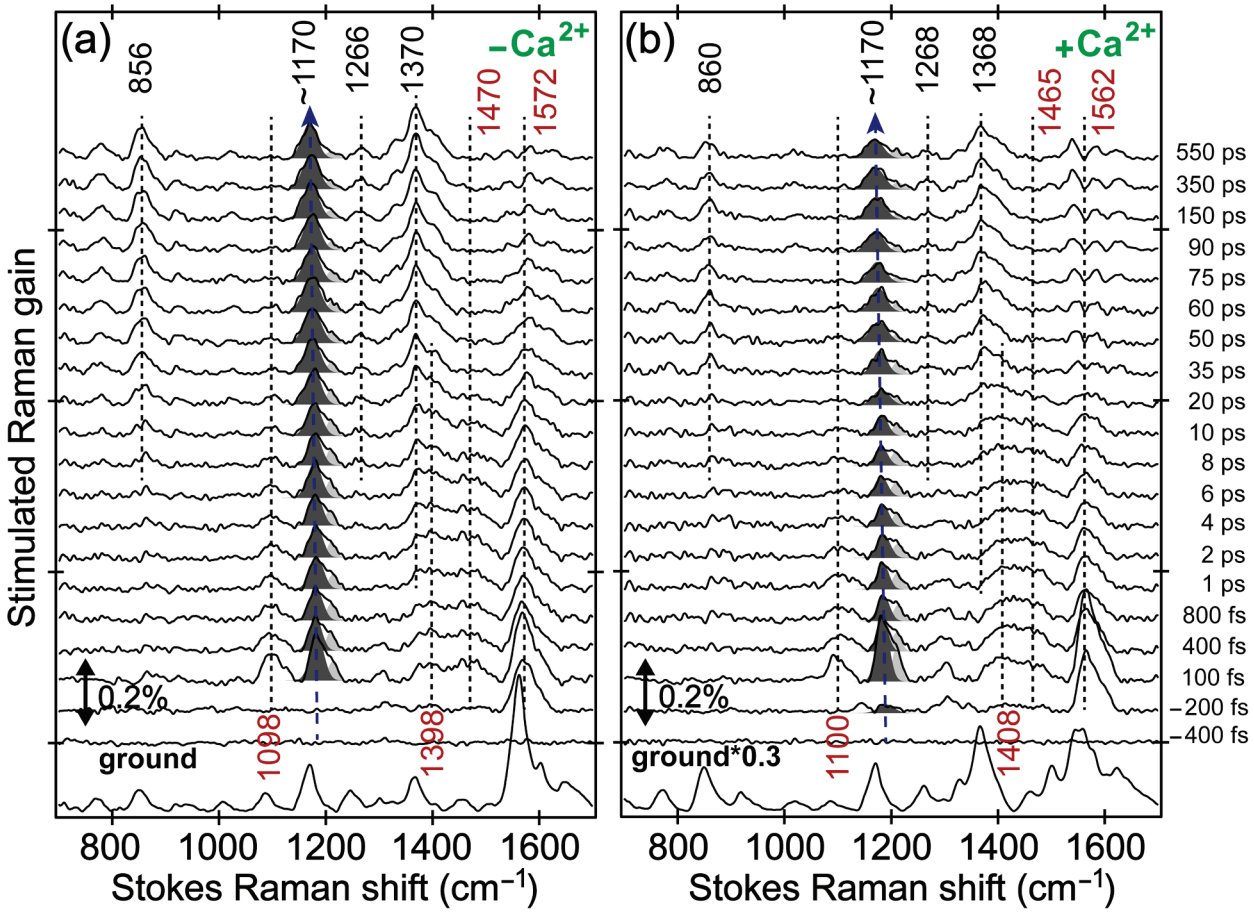

Figure 2. Time-resolved excited-state FSRS of the (a) Ca^{2+}-free and (b) Ca^{2+}-bound G-GECO1.1 biosensor from –400 fs to 550 ps following 400-nm photoexcitation. The Raman pump is at 530 nm. The aqueous-buffer-subtracted S_0 spectra are plotted at the bottom to compare with the S_0-subtracted S_1 spectra. The S_0 spectrum of Ca^{2+}-bound biosensor is multiplied by 0.3. The double-arrowed line represents the stimulated Raman gain of 0.2%. The single-arrowed blue dashed curve indicates the ~1180 cm^{-1} mode (with multi-gaussian least-squares fits shown in dark/light gray shades) frequency redshift toward ~1170 cm^{-1}. The prominent Raman modes in A*/I* are highlighted by vertical dashed lines with their frequencies labeled in red/black, respectively.

We performed DFT calculations on the TYG chromophore *in vacuo* to mimic the relative hydrophobic protein pocket surrounding the chromophore (see Figure 3 insert).[22] The 1180 cm^{-1}

mode mainly consists of the bridge C_7–H rocking with phenol ring-H rocking motion (see Supporting Information, Table S3), which is sensitive to the chromophore two-ring coplanarity change since it involves the ethylenic bridge. In the Ca^{2+}-free biosensor, this pronounced mode redshifts from 1189 to 1172 cm^{-1} with a fitted exponential time constant of 36±2 ps (Figure 3). A smaller redshift from 1185 to 1170 cm^{-1} is observed in the Ca^{2+}-bound biosensor with the time constant of ~60±3 ps. Given that vibrational cooling typically leads to mode frequency blueshift, the structural origin of the observed peak redshift can be revealed by quantum calculations and the general conformational constraints of the chromophore inside the FP pocket.[26,27]

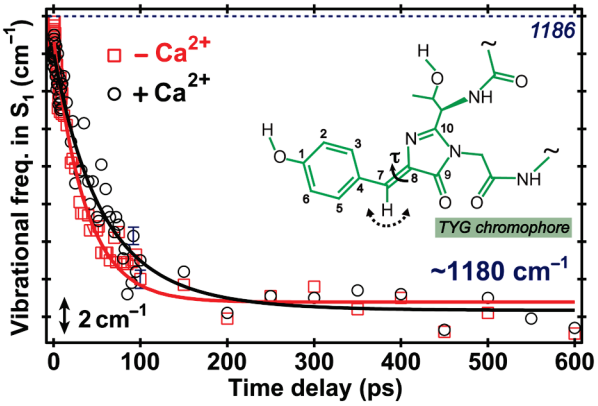

Figure 3. Excited-state vibrational frequency shift of the ~1180 cm^{-1} mode in the Ca^{2+}-free (red) and Ca^{2+}-bound (black) G-GECO1.1 biosensor from 0—600 ps. The Ca^{2+}-free trace is vertically offset by –3 cm^{-1} for comparison. The double-arrowed line indicates a frequency magnitude of 2 cm^{-1}. The bridge C–H rocking motion is depicted with dotted arrows near the TYG chromophore molecular structure in the inset. The τ rotation is shown around the ethylenic double bond. The representative error bars are shown for time-resolved data points at ~100 ps for both samples.

Since the protein matrix provides strategic constraints that effectively inhibit chromophore twisting and increase the fluorescence quantum yield (QY, one of the most important biological

functions and application parameters for these Ca^{2+} biosensors),[28,29] a series of Gaussian-DFT calculations (results tabulated in Supporting Information, Table S4) were performed to infer the effect of protonation and two-ring coplanarity on the observed vibrational mode frequency: protonated/deprotonated chromophore in a coplanar (0°) to 40°-twisted in 10° interval (τ angle, depicted in Figure 3 insert) conformation in S_0. Our previous calculations on an SYG chromophore suggested that a twisting angle of 20° in S_0 can capture the overall frequency shift trend in S_1.[20] Table 1 specifically shows that if the chromophore maintains two-ring coplanarity while undergoing ESPT, the vibrational mode (bridge C_7–H rocking with phenol ring-H rocking) frequency would slightly blueshift by 2 cm^{-1}. However, upon deprotonation with τ=20°, the 1185 cm^{-1} mode redshifts to 1178 cm^{-1}, representing a frequency drop of 7 cm^{-1}. Moreover, ring twist without deprotonation leads to a small blueshift of 1 cm^{-1}. The experimentally observed redshift is 17/15 cm^{-1} in the Ca^{2+}-free/bound biosensor, respectively, consistent with the calculated frequency trend that reflects the chromophore ring twist during the ESPT process from A* to I*.

Table 1. Gaussian-DFT calculation results for the ~1180 cm^{-1} mode of the protonated/deprotonated TYG chromophore in the coplanar and twisted confirmation

Protonated chromophore freq. (cm^{-1})[a]		Deprotonated chromophore freq. (cm^{-1})[a]	
Coplanar	20°-twisted	Coplanar	20°-twisted
1185	1186	1187	1178

[a] The normal mode frequencies are calculated from DFT-RB3LYP calculations of a ground-state geometry-optimized TYG chromophore capped with methyl groups using 6-31G+(d,p) basis sets *in vacuo* and are scaled with a factor of 0.97 (see Supporting Information, Table S4 for an expanded calculation set with systematic variation of the τ angle from 0° to 40°).

Notably, our reported ESPT time constants[16] of ~50/30 ps represent a reversed trend to the time constants attributed to ring twist, i.e., ~36/60 ps for the Ca^{2+}-free/bound biosensor (Figure 3), respectively. The ring twist and ESPT time constants are comparable but with the opposite

trend, suggesting that they compete with each other. We speculate that both processes dissipate photoexcitation energy, and the percentage of each contribution depends on the interplay between chromophore photoacidity, skeletal motions, and local environment.[16,30] Also, the twist-induced mode frequency redshift is larger in Ca^{2+}-free (17 cm^{-1}) than Ca^{2+}-bound (15 cm^{-1}) biosensor. These results infer the structural dynamics basis of the chromophore pocket affected by Ca^{2+} binding at the adjacent CaM domain. Because the Ca^{2+}-free biosensor has a β-barrel opening near the interfacial region between the extended CaM and circularly permuted GFP domains, the chromophore has more freedom to move in a less constrained environment, resulting in faster twisting with larger magnitude. In the Ca^{2+}-bound state, CaM wraps around the M13 peptide and largely shields the β-barrel opening of GFP domain, so the chromophore senses a more restrained environment that leads to slower twisting with smaller magnitude, while ESPT becomes more efficient as the closed-in residue Arg377 increases local hydrophilicity and could potentially help to stabilize the deprotonated chromophore.[16] Regarding pertinent motions that promote ring twist, our DFT calculation shows a ring out-of-plane motion at ~120 cm^{-1} that may be one of several chromophore skeletal motions being coherently excited by the fs 400-nm photoexcitation pulse. These vibrational modes can collectively break the ground-state two-ring coplanarity on the ps timescale in the electronic excited state.[18,20,22]

In comparison to wild-type (wt)GFP with QY≈0.8, the corresponding QY is only 0.20/0.46 for the Ca^{2+}-free/bound G-GECO1.1 biosensor.[12] This may be correlated with the chromophore twist. The wtGFP chromophore is in a highly protected, well-defined H-bonding environment (i.e., with a conserved H_2O molecule above the two-ring plane and within H-bonding distance to the phenolic hydroxyl of the SYG chromophore),[22,31] which governs the chromophore motion to be a specific phenolic-ring wag that facilitates ESPT as the main energy dissipation channel,[22] leading

to high QY. In contrast, the TYG chromophore in G-GECO1.1 has more conformational freedom and solvent exposure due to the β-barrel opening.[8,12] This molecular construct lowers the potential barrier for two-ring twist and makes it a viable channel for energy dissipation following photoexcitation, in competition with ESPT on similar timescales (i.e., tens of ps), leading to lower QY than wtGFP. This argument further supports higher QY in the Ca^{2+}-bound than Ca^{2+}-free G-GECO1.1 because the former chromophore has faster ESPT, slower ring twist, and less solvent exposure. Furthermore, comparison to the GFP chromophore synthetic analogue *p*-hydroxybenzilidene-imidazolinone (HBDI) is useful because the model chromophore undergoes rapid photoinduced ring twisting in solution and is essentially non-fluorescent.[28]

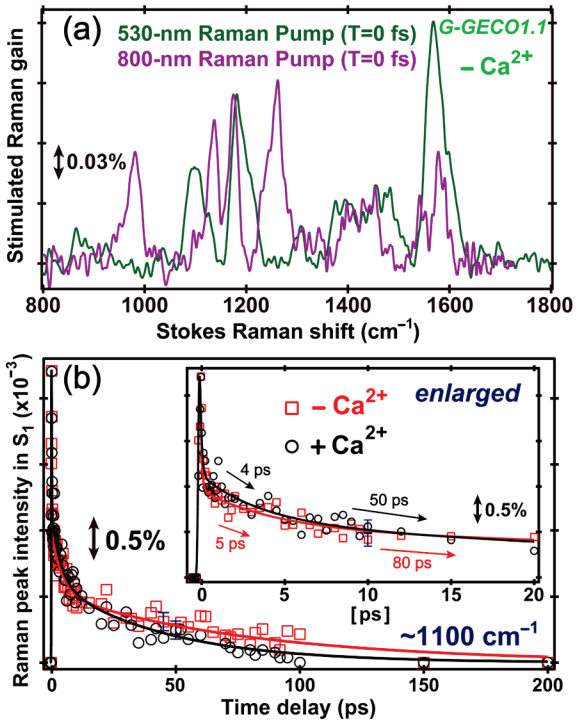

Figure 4. Excited-state Raman spectra and intensity dynamics of the G-GECO1.1 biosensor following 400-nm photoexcitation. (a) Time-zero spectra of the Ca^{2+}-free biosensor chromophore with 530-nm (olive) and 800-nm (magenta) Raman pump. The latter spectrum is multiplied by 5 to match the former spectrum peak intensity at ~1180 cm^{-1}. (b) Time-resolved excited-state

integrated intensity of the 1098/1100 cm^{-1} modes in Ca^{2+}-free (red)/bound (black) G-GECO1.1 with 530-nm Raman pump within 200 ps after photoexcitation. The insert shows an enlarged plot up to 20 ps. Representative error bars (dark blue) are shown for data points at ~50 ps in (b) and 10 ps in the insert, respectively. The least-squares fitted time constants beyond the initial sub-ps peak intensity drop are noted in the insert. The double-arrowed line indicates the Raman gain magnitude. The $+Ca^{2+}$ peak is normalized to the stronger $–Ca^{2+}$ peak with a scaling factor of 1.2.

Figure 4a presents excited-state FSRS data of the Ca^{2+}-free biosensor at photoexcitation time zero with 530 vs. 800-nm Raman pump. The 400-nm pulse mainly pumps the protonated species (A→A*), so at time zero when no significant structural motion can occur, the observed S_1 modes are all A* and their frequencies should match if the sample is homogeneous that leads to the same vibrational energy levels in S_1.[32,33] However, clear spectral differences including frequency shifts indicate that different Raman pump selectively enhances different population of the protein ensemble. In particular, the "protonated" biosensor could have various confirmations at S_0 equilibrium, which can be grouped into the "largely protonated" chromophore (i.e., loosely H-bonded with surrounding partners such as H_2O molecules) and "partially deprotonated" chromophore (i.e., more tightly H-bonded with surrounding partners). Upon 400-nm excitation, these A-species are all pumped to S_1 due to their broad absorption band near 400 nm (see Figure S2), whereas the deprotonated B-species with 500-nm absorption peak cannot be directly excited. Because the 800-nm Raman pump enhances the A* species with largely protonated character due to two-photon absorption[3,16,22,34] whereas the 530-nm Raman pump enhances the A* species with partially deprotonated character,[16] the observed Raman modes in S_1 exhibit marked differences. For example, the much enhanced ~1100, 1470 and 1570 cm^{-1} modes (i.e., they were not observed

with the 800-nm Raman pump,[16] see Table S3 for major atomic motion assignment) are associated with partially deprotonated species in the A* Franck-Condon region. The temporal evolution of these modes dominates the excited-state FSRS dynamics in Figure 2. In contrast, the 800-nm Raman pump ensures that the largely protonated A* species dominates and the associated ESPT time constants (~50/30 ps) should represent the upper limit of proton transfer via higher potential energy barrier crossing inside the G-GECO1.1 biosensor.[16]

Further experimental support for chromophore inhomogeneity can be seen in Figure 4b, which compares the 1098/1100 cm^{-1} mode decay in the Ca^{2+}-free/bound biosensor. Being largely absent in FSRS data with 800-nm Raman pump, this mode with a monotonic decay in Figure 2 supports its assignment to A* species with partially deprotonated chromophore which is specifically enhanced by the 530-nm Raman pump. The fitted mode intensity dynamics reveal three-exponential decay time constants of ~90 fs (79%)/80 fs (73%), 5 ps (10%)/4 ps (13%), and 80 ps (11%)/50 ps (14%) in the Ca^{2+}-free/bound biosensor (fitted amplitude weight), respectively. Beyond the initial sub-ps intensity drop, the two decay components on the ps timescale can be clearly seen in Figure 4b insert. The ~5 ps decay component has not been observed using 800-nm Raman pump, which strongly argues that it is associated with the partially deprotonated A* species that was "hidden" in our previous report.[16] This time constant closely matches solvation process that was observed for photoacid pyranine following the initial charge-separation stage in water,[19,35-37] which can be reasonably assigned to the A subpopulation with deprotonated character in S_0 due to tighter H-bonding configurations. At early time, the proton can shift away from the chromophore via pre-existing H-bonding chain on the ~100 fs timescale with the aforementioned initial intensity drop of PA* modes.[20,38-40] Subsequently, the surrounding H_2O molecules solvate and stabilize the further deprotonated chromophore on the ~5 ps timescale,

insensitive to the Ca^{2+}-binding state. Based on these newly acquired spectral data, we expect that site-specific mutations in the Ca^{2+}-bound protein chromophore pocket that can increase the subpopulation of A with tighter H-bonding configurations should help to improve the biosensor efficiency and/or brightness.[12]

Notably, the retrieved time constants of 80/50 ps are larger than those obtained using the 800-nm Raman pump (50/30 ps) and the 1370 cm^{-1} mode rise dynamics (42/22 ps) for the Ca^{2+}-free/bound biosensor, respectively. For verification of the I* accumulation, we also plotted the rise dynamics of the 860 cm^{-1} mode (Figure S5) and obtained 42/27 ps time constants. Since the 860 or 1370 cm^{-1} mode rise reports on the I* appearance after ~10 ps,[16] it cannot accurately capture the deprotonated species generated on the ~5 ps timescale; instead, it correlates well with the largely protonated A* species following photoexcitation that converts to I* species. For those A* species with partially deprotonated character, the 80/50 ps decay suggests that after initial proton transfer via pre-existing H-bonding chains and the solvation stage, the majority of the chromophores needs to search phase space longer through larger-scale conformational motions such as two-ring twist to further slide down the I* potential energy surface before fluorescence.

In summary, we implemented a wavelength-tunable FSRS setup to observe ultrafast structural evolution of the TYG chromophore inside an intensiometric fluorescent protein-based Ca^{2+} biosensor G-GECO1.1 during photoinduced proton transfer. A two-ring twist out of coplanarity is revealed by the redshift of an excited-state vibrational marker band at ~1180 cm^{-1} mainly involving bridge C–H rock and phenol ring-H rock with time constants of 36/60 ps for the Ca^{2+}-free/bound biosensor, respectively. Due to pre-resonance enhancement, the 530-nm Raman pump allows us to investigate a different species from the ones we studied using 800-nm Raman pump, thus providing deeper insights into ESPT pathways and conformational

inhomogeneity of the biosensor chromophore in its protein pocket. Since the macroscopic functionality of intensiometric biosensors mainly depends on the change of fluorescence quantum yield, our improved understanding of molecular structural dynamics as a competition between ring twist and ESPT on the ps to tens of ps timescale, opens new ways to atomically modify the chromophore and/or site-specifically mutate protein residues around the chromophore to rationally develop protein biosensors for life sciences.

ACKNOWLEDGMENTS

This work was supported by the NSF CAREER Award (CHE-1455353), Oregon State University (OSU) Faculty Research Startup Grant and General Research Fund (to C.F.). We thank Dr. Yongxin Zhao and Prof. Robert E. Campbell from the University of Alberta in Canada for providing the G-GECO1.1 protein biosensor samples. We appreciate the 2014 and 2015 OSU chemistry departmental Dorothy and Ramon Barnes Graduate Fellowship to Y. W. and L. T., and thank Breland Oscar for helpful discussions.

Supporting Information. Tunable FSRS setup, electronic absorption and fluorescence spectroscopy of the Ca^{2+}-free and bound G-GECO1.1 biosensors, effect of the Raman pump wavelength (i.e., 530 and 800 nm) on the ground-state FSRS of biosensors, time-resolved excited-state FSRS data with spectral baselines, S_1 vibrational dynamics of the deprotonated chromophore after ESPT, further discussion on the chromophore inhomogeneity and ring-twisting motion inside the protein pocket, additional Figures S1—S5 and Tables S1—S4. This material is available free of charge via the Internet at http://pubs.acs.org.

AUTHOR INFORMATION

Corresponding Author

*Email: Chong.Fang@oregonstate.edu.

Notes

The authors declare no competing financial interest.

REFERENCES

(1) Shimomura, O.; Johnson, F. H.; Saiga, Y. Extraction, Purification and Properties of Aequorin, a Bioluminescent Protein from the Luminous Hydromedusan, *Aequorea*. *J. Cell. Comp. Physiol*. **1962**, *59*, 223-239.

(2) Chalfie, M.; Tu, Y.; Euskirchen, G.; Ward, W. W.; Prasher, D. C. Green Fluorescent Protein as a Marker for Gene Expression. *Science* **1994**, *263*, 802-805.

(3) Tsien, R. Y. The Green Fluorescent Protein. *Annu. Rev. Biochem*. **1998**, *67*, 509-544.

(4) Hell, S. W.; Wichmann, J. Breaking the Diffraction Resolution Limit by Stimulated Emission: Stimulated-Emission-Depletion Fluorescence Microscopy. *Opt. Lett*. **1994**, *19*, 780-782.

(5) Betzig, E.; Patterson, G. H.; Sougrat, R.; Lindwasser, O. W.; Olenych, S.; Bonifacino, J. S.; Davidson, M. W.; Lippincott-Schwartz, J.; Hess, H. F. Imaging Intracellular Fluorescent Proteins at Nanometer Resolution. *Science* **2006**, *313*, 1642-1645.

(6) Jung, G., (Ed.) *Fluorescent Proteins II: Application of Fluorescent Protein Technology*; Springer-Verlag: Berlin Heidelberg, 2012; Vol. 12.

(7) Miyawaki, A.; Llopis, J.; Heim, R.; McCaffery, J. M.; Adams, J. A.; Ikura, M.; Tsien, R. Y. Fluorescent Indicators for Ca^{2+} Based on Green Fluorescent Proteins and Calmodulin. *Nature* **1997**, *388*, 882-887.

(8) Akerboom, J.; Rivera, J. D. V.; Guilbe, M. M. R.; Malavé, E. C. A.; Hernandez, H. H.; Tian, L.; Hires, S. A.; Marvin, J. S.; Looger, L. L.; Schreiter, E. R. Crystal Structures of the GCaMP Calcium Sensor Reveal the Mechanism of Fluorescence Signal Change and Aid Rational Design. *J. Biol. Chem.* **2009**, *284*, 6455-6464.

(9) Berg, J.; Hung, Y. P.; Yellen, G. A Genetically Encoded Fluorescent Reporter of ATP:ADP Ratio. *Nat. Methods* **2009**, *6*, 161-166.

(10) Prevarskaya, N.; Skryma, R.; Shuba, Y. Calcium in Tumour Metastasis: New Roles for Known Actors. *Nat. Rev. Cancer* **2011**, *11*, 609-618.

(11) Grienberger, C.; Konnerth, A. Imaging Calcium in Neurons. *Neuron* **2012**, *73*, 862-885.

(12) Zhao, Y.; Araki, S.; Wu, J.; Teramoto, T.; Chang, Y.-F.; Nakano, M.; Abdelfattah, A. S.; Fujiwara, M.; Ishihara, T.; Nagai, T.; et al. An Expanded Palette of Genetically Encoded Ca^{2+} Indicators. *Science* **2011**, *333*, 1888-1891.

(13) Akerboom, J.; Chen, T.-W.; Wardill, T. J.; Tian, L.; Marvin, J. S.; Mutlu, S.; Calderón, N. C.; Esposti, F.; Borghuis, B. G.; Sun, X. R.; et al. Optimization of a GCaMP Calcium Indicator for Neural Activity Imaging. *J. Neurosci.* **2012**, *32*, 13819-13840.

(14) Yamada, Y.; Mikoshiba, K. Quantitative Comparison of Novel GCaMP-type Genetically Encoded Ca^{2+} Indicators in Mammalian Neurons. *Front. Cell. Neurosci.* **2012**, *6*, 41.

(15) Chen, Y.; Song, X.; Ye, S.; Miao, L.; Zhu, Y.; Zhang, R.-G.; Ji, G. Structural Insight into Enhanced Calcium Indicator GCaMP3 and GCaMPJ to Promote Further Improvement. *Protein Cell* **2013**, *4*, 299-309.

(16) Tang, L.; Liu, W.; Wang, Y.; Zhao, Y.; Oscar, B. G.; Campbell, R. E.; Fang, C. Unraveling Ultrafast Photoinduced Proton Transfer Dynamics in a Fluorescent Protein Biosensor for Ca^{2+} Imaging. *Chem. Eur. J.* **2015**, *21*, 6481-6490.

(17) Frontiera, R. R.; Fang, C.; Dasgupta, J.; Mathies, R. A. Probing Structural Evolution along Multidimensional Reaction Coordinates with Femtosecond Stimulated Raman Spectroscopy. *Phys. Chem. Chem. Phys.* **2012**, *14*, 405-414.

(18) Liu, W.; Han, F.; Smith, C.; Fang, C. Ultrafast Conformational Dynamics of Pyranine during Excited State Proton Transfer in Aqueous Solution Revealed by Femtosecond Stimulated Raman Spectroscopy. *J. Phys. Chem. B* **2012**, *116*, 10535-10550.

(19) Han, F.; Liu, W.; Fang, C. Excited-State Proton Transfer of Photoexcited Pyranine in Water Observed by Femtosecond Stimulated Raman Spectroscopy. *Chem. Phys.* **2013**, *422*, 204-219.

(20) Wang, Y.; Tang, L.; Liu, W.; Zhao, Y.; Oscar, B. G.; Campbell, R. E.; Fang, C. Excited State Structural Events of a Dual-Emission Fluorescent Protein Biosensor for Ca^{2+} Imaging Studied by Femtosecond Stimulated Raman Spectroscopy. *J. Phys. Chem. B* **2015**, *119*, 2204-2218.

(21) Myers, A. B.; Mathies, R. A. Resonance Raman intensities: A Probe of Excited-State Structure and Dynamics. In *Biological Applications of Raman Spectroscopy*; Spiro, T. G., Ed.; John Wiley & Sons, Inc.: New York, 1987; Vol. 2; pp 1-58.

(22) Fang, C.; Frontiera, R. R.; Tran, R.; Mathies, R. A. Mapping GFP Structure Evolution during Proton Transfer with Femtosecond Raman Spectroscopy. *Nature* **2009**, *462*, 200-204.

(23) Zhu, L.; Liu, W.; Fang, C. A Versatile Femtosecond Stimulated Raman Spectroscopy Setup with Tunable Pulses in the Visible to Near Infrared. *Appl. Phys. Lett.* **2014**, *105*, 041106.

(24) Chattoraj, M.; King, B. A.; Bublitz, G. U.; Boxer, S. G. Ultra-Fast Excited State Dynamics in Green Fluorescent Protein: Multiple States and Proton Transfer. *Proc. Natl. Acad. Sci. U.S.A.* **1996**, *93*, 8362-8367.

(25) Frisch, M. J.; Trucks, G. W.; Schlegel, H. B.; Scuseria, G. E.; Robb, M. A.; Cheeseman, J. R.; Scalmani, G.; Barone, V.; Mennucci, B.; Petersson, G. A.; et al. Gaussian 09, Revision B.1; Gaussian, Inc.: Wallingford, CT, 2009.

(26) Zimmer, M. Green Fluorescent Protein (GFP): Applications, Structure, and Related Photophysical Behavior. *Chem. Rev.* **2002**, *102*, 759-781.

(27) Maddalo, S. L.; Zimmer, M. The Role of the Protein Matrix in Green Fluorescent Protein Fluorescence. *Photochem. Photobiol.* **2006**, *82*, 367-372.

(28) Vengris, M.; van Stokkum, I. H. M.; He, X.; Bell, A. F.; Tonge, P. J.; van Grondelle, R.; Larsen, D. S. Ultrafast Excited and Ground-State Dynamics of the Green Fluorescent Protein Chromophore in Solution. *J. Phys. Chem. A* **2004**, *108*, 4587-4598.

(29) Rafiq, S.; Rajbongshi, B. K.; Nair, N. N.; Sen, P.; Ramanathan, G. Excited State Relaxation Dynamics of Model Green Fluorescent Protein Chromophore Analogs: Evidence for Cis-Trans Isomerism. *J. Phys. Chem. A* **2011**, *115*, 13733-13742.

(30) Oscar, B. G.; Liu, W.; Zhao, Y.; Tang, L.; Wang, Y.; Campbell, R. E.; Fang, C. Excited-State Structural Dynamics of a Dual-Emission Calmodulin-Green Fluorescent Protein Sensor for Calcium Ion Imaging. *Proc. Natl. Acad. Sci. U.S.A.* **2014**, *111*, 10191-10196.

(31) Brejc, K.; Sixma, T. K.; Kitts, P. A.; Kain, S. R.; Tsien, R. Y.; Ormö, M.; Remington, S. J. Structural Basis for Dual Excitation and Photoisomerization of the *Aequorea victoria* Green Fluorescent Protein. *Proc. Natl. Acad. Sci. U.S.A.* **1997**, *94*, 2306-2311.

(32) Fang, C.; Senes, A.; Cristian, L.; DeGrado, W. F.; Hochstrasser, R. M. Amide Vibrations Are Delocalized Across the Hydrophobic Interface of a Transmembrane Helix Dimer. *Proc. Natl. Acad. Sci. U.S.A.* **2006**, *103*, 16740-16745.

(33) Wang, Y.; Liu, W.; Tang, L.; Oscar, B. G.; Han, F.; Fang, C. Early Time Excited-State Structural Evolution of Pyranine in Methanol Revealed by Femtosecond Stimulated Raman Spectroscopy. *J. Phys. Chem. A* **2013**, *117*, 6024-6042.

(34) Drobizhev, M.; Makarov, N. S.; Tillo, S. E.; Hughes, T. E.; Rebane, A. Two-Photon Absorption Properties of Fluorescent Proteins. *Nat. Meth.* **2011**, *8*, 393-399.

(35) Tran-Thi, T.-H.; Gustavsson, T.; Prayer, C.; Pommeret, S.; Hynes, J. T. Primary Ultrafast Events Preceding the Photoinduced Proton Transfer from Pyranine to Water. *Chem. Phys. Lett.* **2000**, *329*, 421-430.

(36) Leiderman, P.; Genosar, L.; Huppert, D. Excited-State Proton Transfer: Indication of Three Steps in the Dissociation and Recombination Process. *J. Phys. Chem. A* **2005**, *109*, 5965-5977.

(37) Spry, D. B.; Goun, A.; Fayer, M. D. Deprotonation Dynamics and Stokes Shift of Pyranine (HPTS). *J. Phys. Chem. A* **2007**, *111*, 230-237.

(38) Tolbert, L. M.; Solntsev, K. M. Excited-State Proton Transfer: From Constrained Systems to "Super" Photoacids to Superfast Proton Transfer. *Acc. Chem. Res.* **2002**, *35*, 19-27.

(39) Mohammed, O. F.; Dreyer, J.; magnes, B.-Z.; Pines, E.; Nibbering, E. T. J. Solvent-Dependent Photoacidity State of Pyranine Monitored by Transient Mid-Infrared Spectroscopy. *ChemPhysChem* **2005**, *6*, 625-636.

(40) Simkovitch, R.; Shomer, S.; Gepshtein, R.; Huppert, D. How Fast Can a Proton-Transfer Reaction Be beyond the Solvent-Control Limit? *J. Phys. Chem. B* **2015**, *119*, 2253-2262.

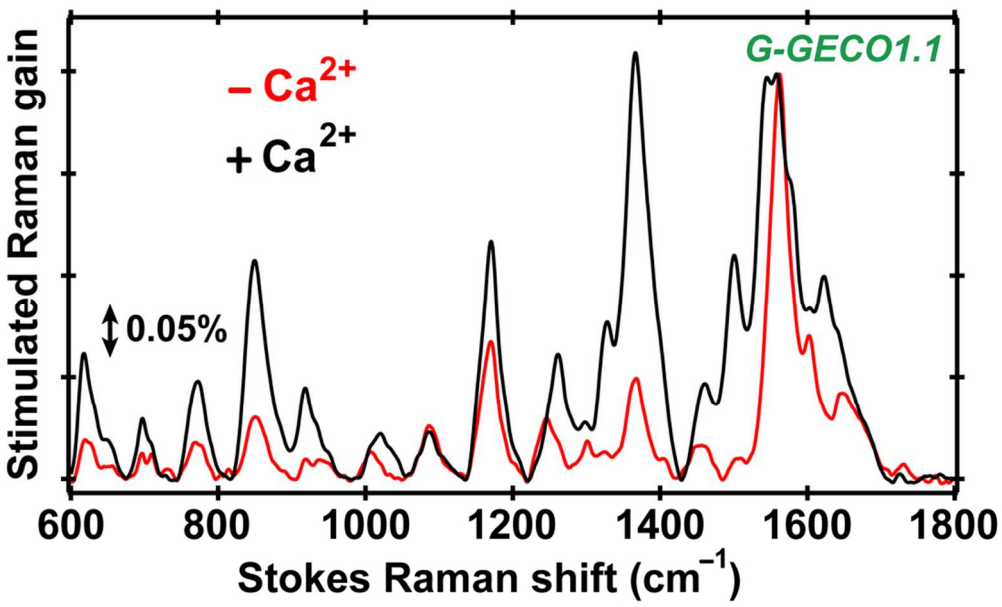

Figure 1. Ground-state FSRS of the G-GECO1.1 biosensor with 530-nm Raman pump.
46x27mm (600 x 600 DPI)

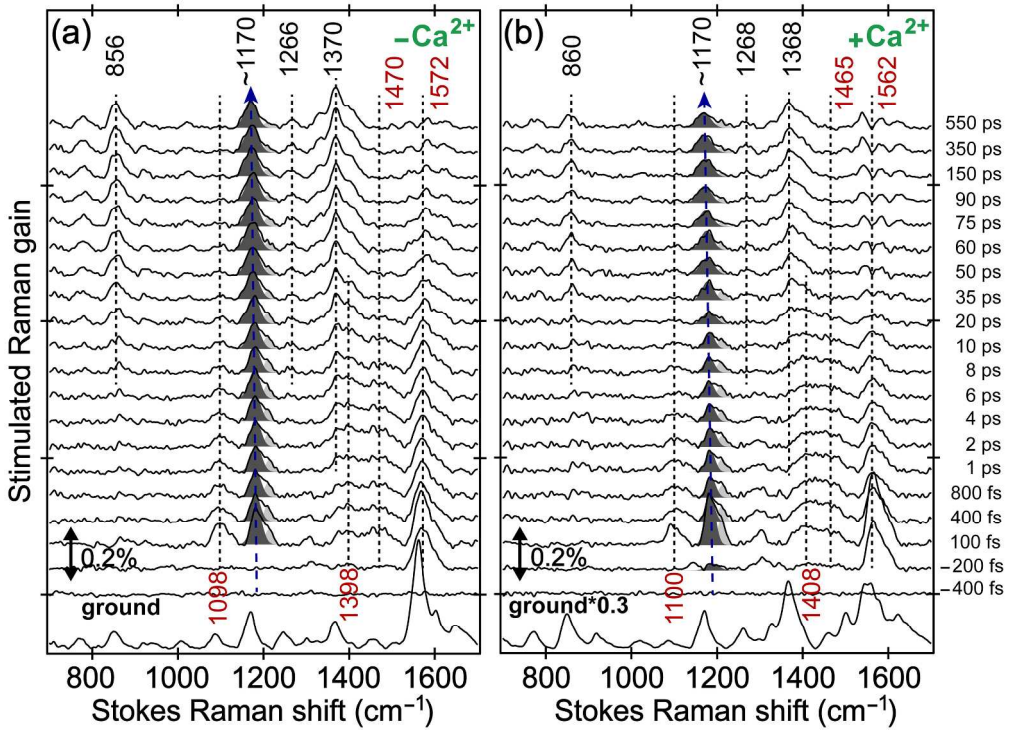

Figure 2. Time-resolved excited-state FSRS of the (a) Ca^{2+}-free and (b) Ca^{2+}-bound G-GECO1.1 biosensor from –400 fs to 550 ps following 400-nm photoexcitation.
122x89mm (600 x 600 DPI)

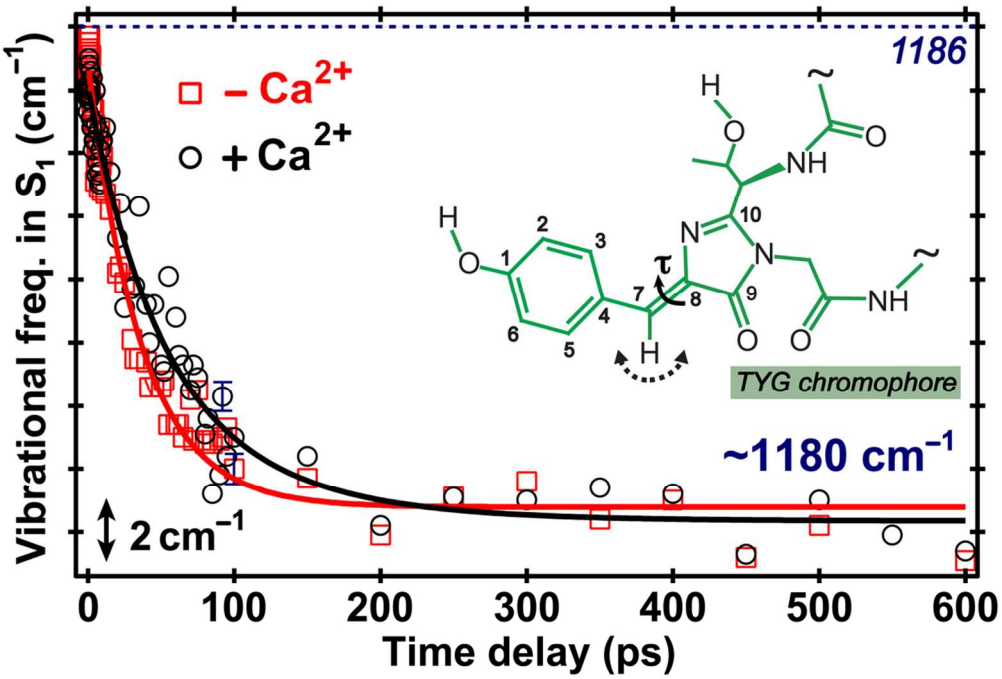

Figure 3. Excited-state vibrational frequency shift of the ~1180 cm^{-1} mode in the Ca^{2+}-free (red) and Ca^{2+}-bound (black) G-GECO1.1 biosensor from 0—600 ps.
52x35mm (600 x 600 DPI)

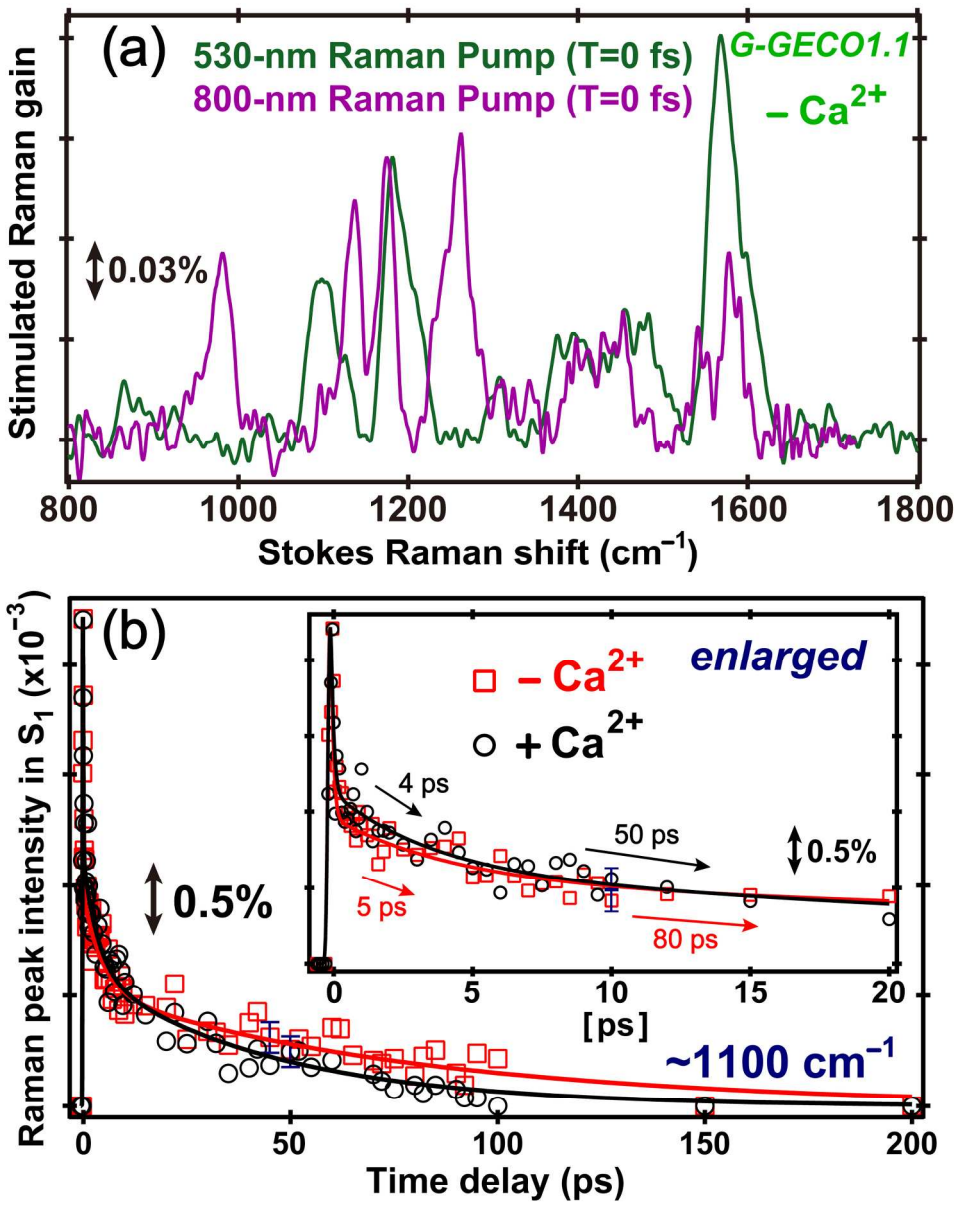

Figure 4. Excited-state Raman spectra and intensity dynamics of the G-GECO1.1 biosensor following 400-nm photoexcitation.
94x119mm (600 x 600 DPI)

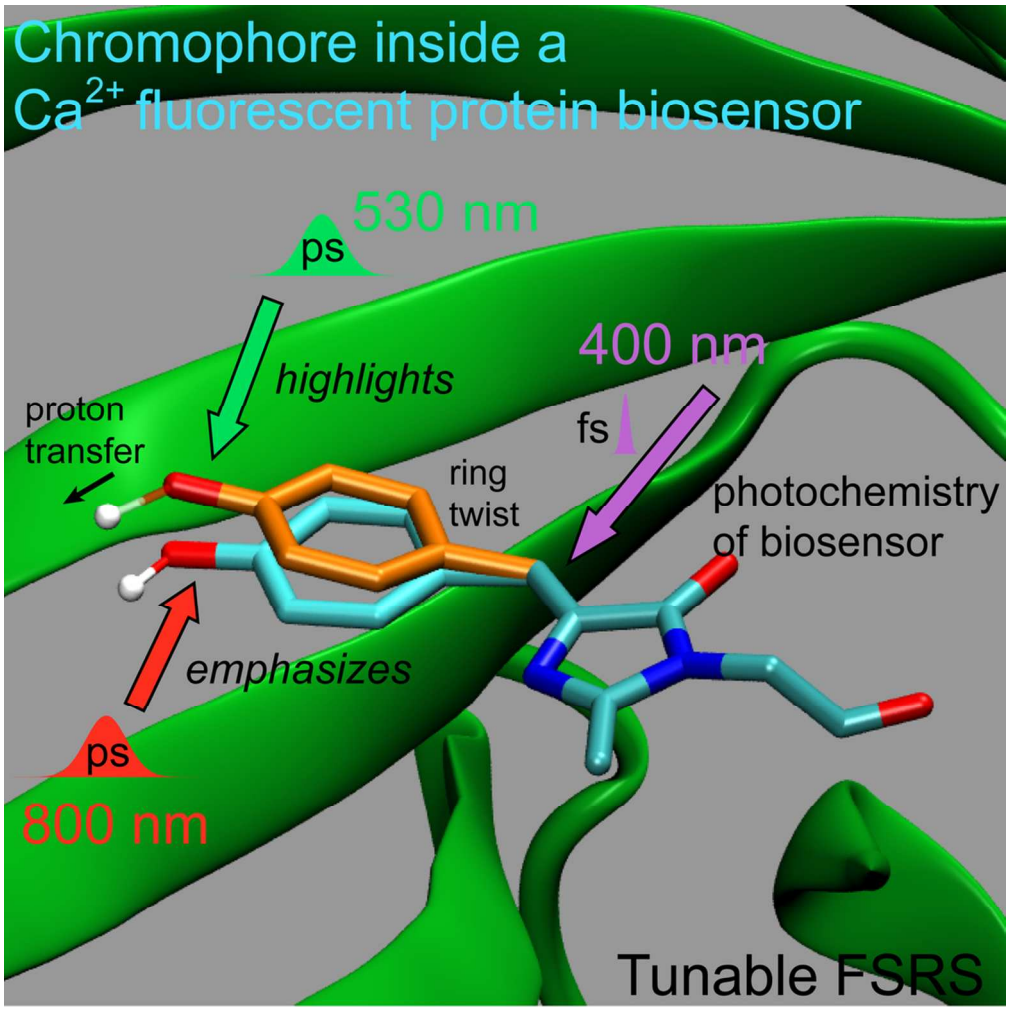

TOC Graphic
49x49mm (600 x 600 DPI)